Available online at www.sciencedirect.com
SCIENCE DIRECT
Journal of Sound and Vibration 294 (2006) 585–595
JOURNAL OF SOUND AND VIBRATION
www.elsevier.com/locate/jsvi

Short Communication

Chaos and transient chaos in an experimental nonlinear pendulum

Aline Souza de Paula, Marcelo Amorim Savi*, Francisco Heitor Iunes Pereira-Pinto

COPPE - Department of Mechanical Engineering, Universidade Federal do Rio de Janeiro, P.O. Box 68.503, 21.941.972 Rio de Janeiro, RJ, Brazil

Received 15 April 2005; received in revised form 21 October 2005; accepted 11 November 2005
Available online 18 January 2006

Abstract

Pendulum is a mechanical device that instigates either technological or scientific studies, being associated with the measure of time, stabilization devices as well as ballistic applications. Nonlinear characteristic of the pendulum attracts a lot of attention being used to describe different phenomena related to oscillations, bifurcation and chaos. The main purpose of this contribution is the analysis of chaos in an experimental nonlinear pendulum. The pendulum consists of a disc with a lumped mass that is connected to a rotary motion sensor. This assembly is driven by a string–spring device that is attached to an electric motor and also provides torsional stiffness to the system. A magnetic device provides an adjustable dissipation of energy. This experimental apparatus is modeled and numerical simulations are carried out. Free and forced vibrations are analyzed showing that numerical results are in close agreement with those obtained from experimental data. This analysis shows that the experimental pendulum has a rich response, presenting periodic response, chaos and transient chaos.

1. Introduction

Chaotic behavior of physical systems has been extensively analyzed from the early sixties when E. Lorenz develops studies on the unpredictability of meteorological phenomena. Nowadays, different fields of sciences have special interest in this kind of phenomenon as for example engineering, medicine, ecology, biology and economy.

Mechanical sciences are also included in these areas presenting different situations where chaos appears. Nonlinear pendulum is a mechanical device that attracts a lot of attention being used to describe different phenomena related to oscillations, bifurcation and chaos. Actually, pendulum instigates either technological or scientific studies, being associated with the measure of time, stabilization devices as well as ballistic applications. As a matter of fact, the interest in the study of pendulum motion is old. Galileo (1564–1642) dedicates many efforts to the pendulum analysis where its use should be pointed out for the measure of time. Foucault (1819–1868) presents the first evidence that earth rotates on its axis using a pendulum. It was

*Corresponding author.
E-mail address: savi@ufrj.br (M.A. Savi).

0022-460X/$ - see front matter © 2006 Elsevier Ltd. All rights reserved.
doi:10.1016/j.jsv.2005.11.015

constructed by suspending a pendulum on a long wire from the dome of the Pantheon in Paris. During the history, many studies are carried out analyzing the pendulum dynamics and, certainly, pendulum becomes one of the paradigms in the study of physics and natural phenomena [1].

Regarding the experimental point of view, it is possible to say that experimental findings do not precede theoretical development of nonlinear sciences [2]. However, by observing the words of Poincaré, a pioneer on the nonlinear dynamics and chaos, "*experiment is the sole source of truth*", it is possible to argue that experimental approach tends to grow in nonlinear sciences evaluating different details of the so-called chaos theory. By examining the literature related to experimental analysis of nonlinear pendulum, different mechanical and electrical devices are proposed in order to describe the main characteristics of the pendulum motion [3–6]. Nevertheless, this experimental analysis is complex, especially when it deals with mechanical systems.

The main purpose of this contribution is the analysis of chaos in an experimental nonlinear pendulum. The experimental apparatus was previously presented in Refs. [3,7]. This pendulum has both torsional stiffness and damping. Franca and Savi [8] treat the dynamics of this pendulum in the framework of time-series analysis. Pinto and Savi [9] investigate the signal prediction while Pereira-Pinto et al. [10,11] discuss its chaos control. Here, this problem is revisited exploiting details of its nonlinear dynamics. Essentially, experimental apparatus is modeled and numerical simulations are carried out allowing a comparison with experimental data. Results show that they are in close agreement presenting a rich response which includes chaos and transient chaos.

2. Experimental apparatus and mathematical model

Consider the experimental nonlinear pendulum which is shown in Fig. 1. The right-hand side presents the experimental apparatus while the left-hand side shows its schematic picture. Basically, the pendulum consists of an aluminum disc (1) with a lumped mass (2) that is connected to a rotary motion sensor (4), PASCO CI-6538, which has a precision of $\pm 0.25^{\circ}$, maximum velocity of 30 revolutions/s and maximum sampling frequency of 1000 Hz. This assembly is driven by a string-spring device (6) that is attached to an electric motor (7) (PASCO ME-8750 with 0–12 eV, 0–0.3 A) and also provides torsional stiffness to the system. A magnetic device (3) provides an adjustable dissipation of energy.

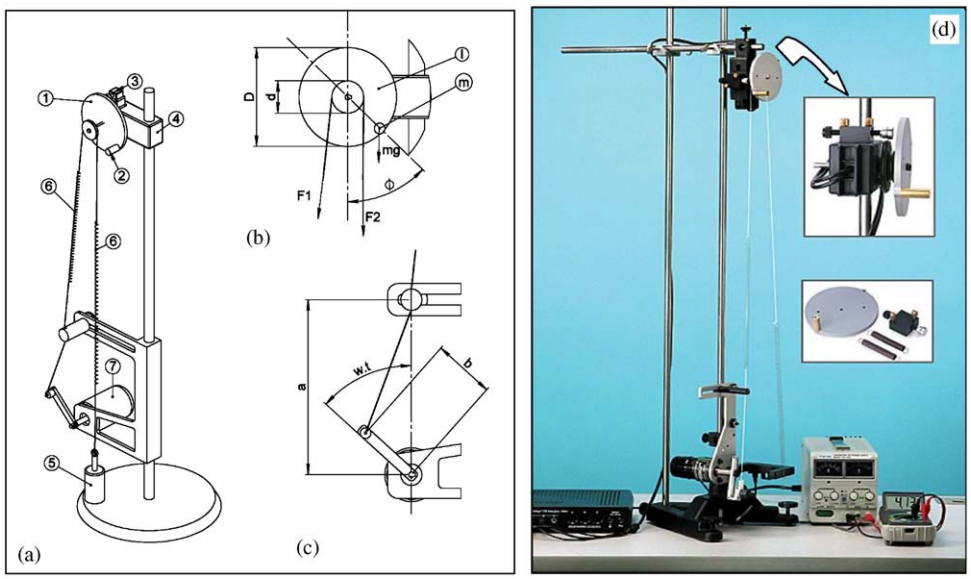

Fig. 1. Nonlinear pendulum: (a) physical model—(1) metallic disc; (2) lumped mass; (3) magnetic damping device; (4) rotary motion sensor (PASCO CI-6538); (5) anchor mass; (6) string–spring device; (7) electric motor (PASCO ME-8750). (b) Parameters and forces on the metallic disc. (c) Parameters from driving device. (d) Experimental apparatus.

2.1. Mathematical model

In order to obtain the equations of motion of the experimental nonlinear pendulum it is assumed that system dissipation may be expressed by a combination of a linear viscous dissipation together with dry friction. Therefore, denoting the angular position as, ϕ, the following equation is obtained:

$$\ddot{\phi} + \frac{\zeta}{I}\dot{\phi} + \frac{kd^2}{2I}\phi + \frac{\mu \operatorname{sgn}(\dot{\phi})}{I} + \frac{mgD \sin(\phi)}{2I} = \frac{kd}{2I}\left(\sqrt{a^2 + b^2 - 2ab\cos(\omega t)} - (a-b)\right), \tag{1}$$

where ω is the forcing frequency related to the motor rotation, a defines the position of the guide of the string with respect to the motor, b is the length of the excitation crank of the motor, D is the diameter of the metallic disc and d is the diameter of the driving pulley, m is the lumped mass, ζ represents the linear viscous damping coefficient, while μ is the dry friction coefficient; g is the gravity acceleration, I is the inertia of the disk-lumped mass and k is the string stiffness. Moreover, $\operatorname{sgn}(x)$ is the sign of the variable x.

In order to model the dry friction in a continuous form, the following relation is used [12]:

$$\mu \operatorname{sgn}(\dot{\phi}) = \frac{2}{\pi}\mu \arctan(q\dot{\phi}), \tag{2}$$

where q assumes a great value, for example, $q = 10^6$. The equation of motion may be written in terms of a first-order differential equations system with the form, $\dot{x} = f(x,t)$, $x \in R^2$. It should be pointed out that the system dynamics depends on the position of the motor rotating crank. The angular position is measured from the vertical position of the crank, being positive when rotating in a counter-clockwise direction. Therefore, it is interesting to identify the position of the rotating crank, calling this as motor phase, θ.

2.2. Parameters identification

Geometrical properties of the pendulum may be easily measured, and the following values are obtained: $a = 1.6 \times 10^{-1}$ m; $b = 6.0 \times 10^{-2}$ m; $d = 4.8 \times 10^{-2}$ m; $D = 9.5 \times 10^{-2}$ m. The lumped mass can be measured with a weight scale, and it is identified as $m = 1.47 \times 10^{-2}$ kg.

After that, it is possible to identify inertia of this system by evaluating the dynamics of the disc subjected to a known torque. Basically, the experimental procedure considers a mass attached to a string that is rolled up in a pulley, attached to a rotary sensor. Suddenly, the mass is released from the equilibrium, subjected to the action of gravity. Assuming a mass of 1.47×10^{-2} kg and a pulley with radius 1.45×10^{-2} m, it is possible to estimate the inertia as $I_{\text{disc}} = mgr/\ddot{\phi}$. Since the value of the acceleration measured from the rotary sensor is $\ddot{\phi} = 24.6\,\text{rad/s}^2$ and $g = 9.81\,\text{m/s}^2$, one concludes that $I_{\text{disc}} = 1.407 \times 10^{-4}\,\text{kg m}^2$. Now, it is possible to estimate the inertia of the disc-lumped mass system considering that $I = mD^2/4 + I_{\text{disc}} = 1.738 \times 10^{-4}\,\text{kg m}^2$.

The spring stiffness is evaluated as the slope of a force–displacement curve, plotted with the aid of two sensors: the rotary sensor shown in Fig. 1 and a force sensor (PS-2104), which has a range of ± 50 N, with 1% of accuracy and resolution of 0.03 N. This procedure identifies springs with $k = 2.47\,\text{N/m}$.

Since the system dissipation characteristics are due to linear viscous damping and also due to dry friction, different procedures must be employed in order to estimate dissipation parameters. Basically, the free response of the pendulum is analyzed, assuming $(\phi, \dot{\phi}) = (\pi/2, 0)$ as initial condition and phase angle $\theta = 0$. In general, it is observed that for the beginning of the motion, when velocities are greater, linear viscous damping is preponderant. As time increases, and the velocity decreases, dry friction becomes more important. Therefore, dissipation parameters are evaluated considering logarithmic decrement procedure for the first part of the movement, while the second part assumes that the differences between two consecutive peaks have a linear decrement. Measuring the decay in the first part, one obtains $\xi = 0.017$ and therefore, $\zeta = 2\xi I\omega_0 = 2.368 \times 10^{-5}\,\text{kg m}^2/\text{s}$. For the second part of the oscillation, it is measured the difference between two consecutive peaks $\Delta x = 0.0525$ and therefore $\mu = (k_0/4)\,\Delta x = 1.272 \times 10^{-4}$ Nm. Here k_0 is related to the linearized stiffness of the system, $k_0 = (kd^2 + mgD)/2$.

3. Free response

In order to start the analysis of the nonlinear experimental pendulum dynamics, free response is focused on. The classical fourth-order Runge–Kutta method is employed for all numerical simulations. The point $\bar{x}$ is an equilibrium point of the system $\dot{x} = f(x)$, if $f(\bar{x}) = 0$. Moreover, the system dynamics in the neighborhood of a point may be analyzed by the eigenvalues of the Jacobian matrix, $A = Df$. Therefore, from equations of motion it is possible to conclude that the number and also the characteristics of the equilibrium points of the experimental pendulum depends on the motor phase, θ. Fig. 2 presents a picture related to these equilibrium points, obtained by analytical and experimental approaches. It shows that the system has only one stable point for small values of θ, a stable spiral, and the same behavior for higher values ($0 < \theta < 2.17$ and $4.11 < \theta < 2\pi$). However, for intermediate values ($2.17 \leqslant \theta \leqslant 4.11$), there are three equilibrium points. For those, two are stable (stable spiral) and the other is unstable, a saddle node.

These results may be confirmed by considering the pendulum free response for different initial conditions and also motor phase. Fig. 3 presents some of these responses, showing the stable equilibrium points depending on the motor phase. Basically, two different motor phases are considered: $\theta = \pi$ and $\pi/2$. Note that for $\theta = \pi$, there are two stable spiral responses and, between these points, there is an unstable point (not shown). On the other hand, for $\theta = \pi/2$, there is only a single stable spiral equilibrium point.

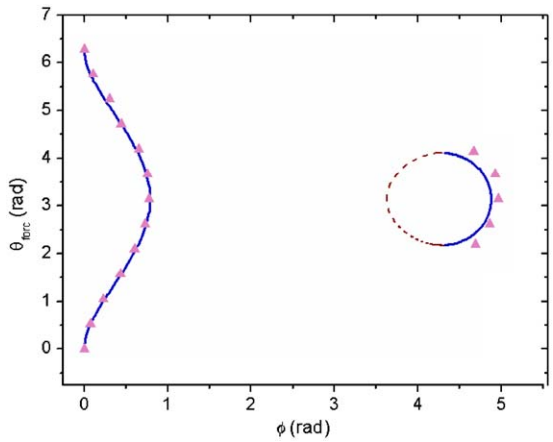

Fig. 2. Equilibrium points map. — stable spiral, - - - saddle, ▲ experimental points.

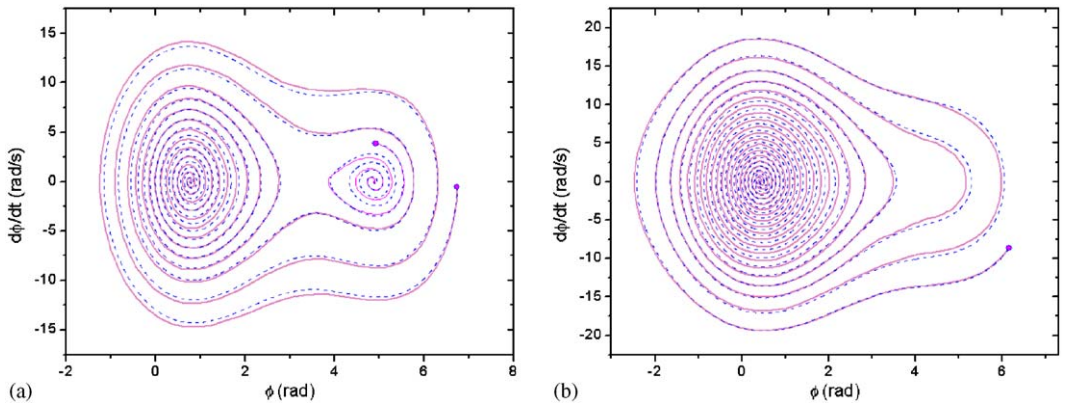

Fig. 3. Free responses for different initial conditions and different value of θ, — experimental, - - - numerical. (a) $\theta = \pi$; (b) $\theta = \pi/2$.

4. Forced response

Forced response of the experimental pendulum is much more complex. In order to perform a global analysis of different kinds of response, bifurcation diagram is constructed, sampling angular position against the slow quasi-static variation of the forcing frequency parameter. Basically, this diagram is constructed by assuming similar initial condition for each parameter value, neglecting the first 2000 periods. This procedure is carried out numerically and confirmed with experiments in some frequencies (Fig. 4). This diagram allows one to observe regions related to periodic and chaotic motion.

Now, different kinds of response are considered, comparing numerical results with those obtained experimentally. Fig. 5 shows periodic responses for different forcing frequency: $\omega = 3.59\,\mathrm{rad/s}$ and $\omega = 5.1\,\mathrm{rad/s}$. It should be pointed out the close agreement between numerical and experimental results. By changing the forcing frequency for $\omega = 5.61\,\mathrm{rad/s}$, a value inside a chaotic region of the bifurcation diagram, chaos appears. Fig. 6 presents state space for both numerical and experimental results, showing again, a close agreement. Lyapunov exponents assure the conclusion about chaotic response. Employing the algorithm due to Wolf et al. [13], the spectrum is $\lambda = (+0.4483, -0.5732)$.

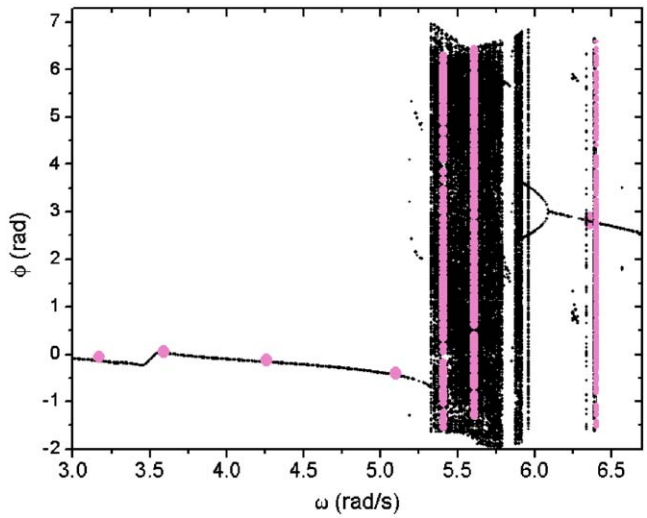

Fig. 4. Bifurcation diagram: ● experimental, ● numerical.

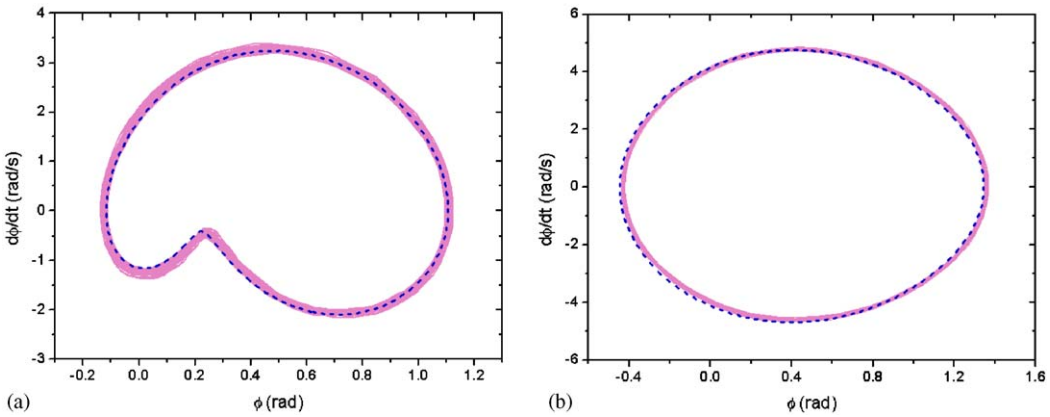

Fig. 5. Periodic forced response for different forcing frequency, — experimental. - - - numerical: (a) $\omega = 3.59\,\mathrm{rad/s}$; (b) $\omega = 5.1\,\mathrm{rad/s}$.

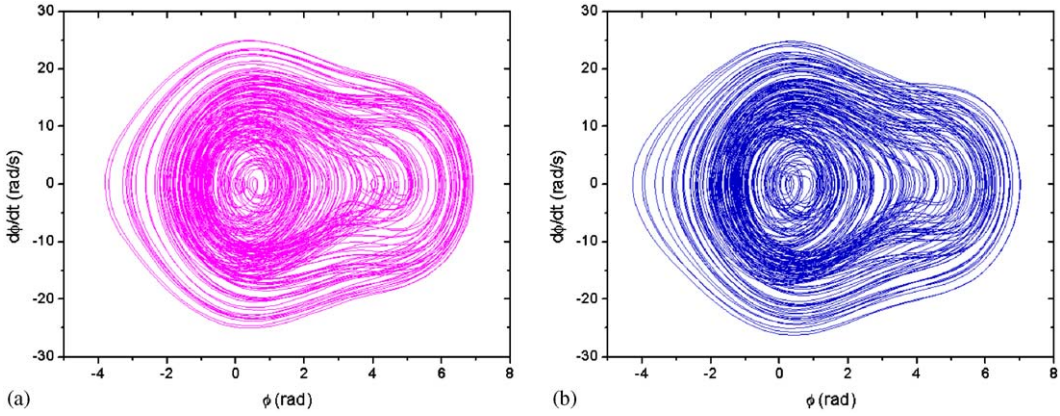

Fig. 6. Chaotic response for $\omega = 5.61$ rad/s: (a) experimental; (b) numerical.

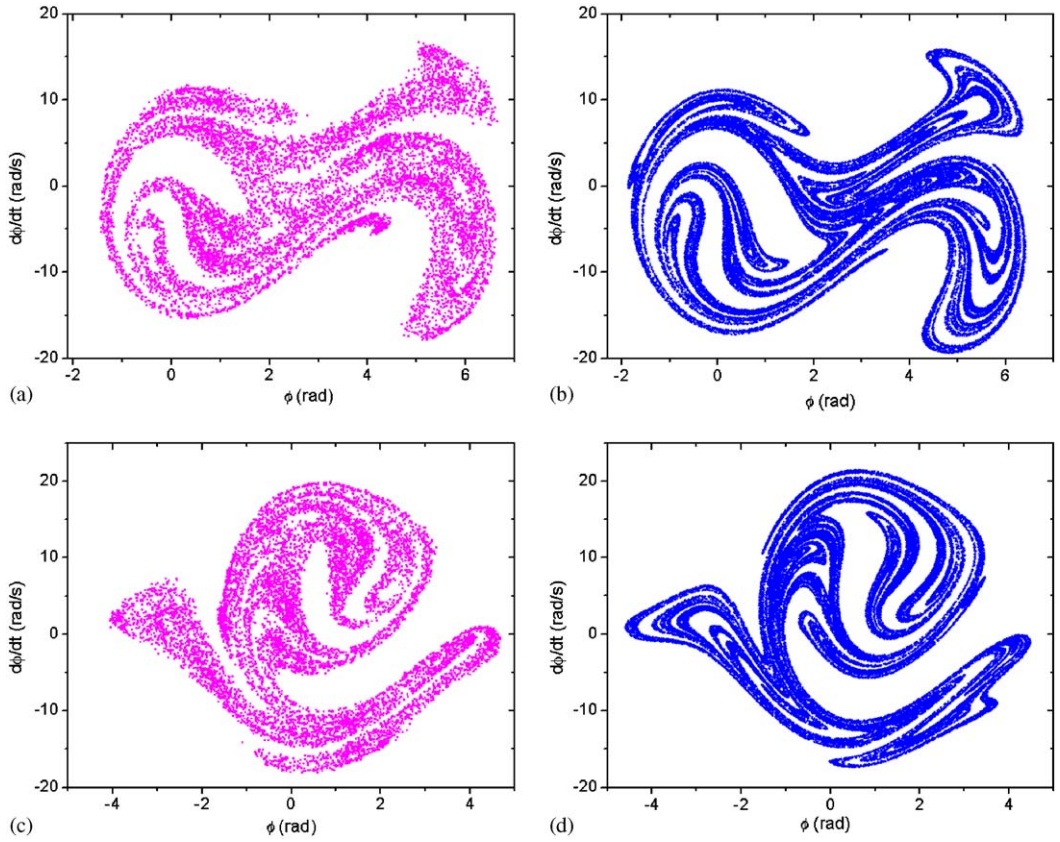

Fig. 7. Strange attractors for $\omega = 5.61$ rad/s: (a, c) experimental; (b, d) numerical.

Poincaré section is a procedure which eliminates time variable by sampling state variables at a rate equal to the forcing period. Basically, it shows the intersections of the orbit with a plane, and chaotic attractor is usually strange in the sense that has a non-integer dimension [14]. Fig. 7 presents both experimental and numerical strange attractors, considering different positions of the section, separated by π. Experimental construction is done considering an analysis of the time series, sampling its values when it crosses a defined surface. The definition of the surface is done considering a signal related to the motor position which is

obtained with the aid of a rotary sensor, similar to the one used to measure the pendulum position. A good agreement between numerical and experimental strange attractors is noticeable.

A geometrical form to understand chaos is related to a transformation known as Smale horseshoe. Basically, it establishes a sequence of contraction–expansion–folding which causes the existence of an infinite number of unstable periodic orbits (UPOs) embedded in a strange attractor [15,16]. Here, the close return method [17] is employed in order to evaluate the UPOs embedded in the experimental strange attractor discussed in Fig. 7. Fig. 8 shows some orbits identified in the attractor employing the cited close return method. On the other hand, Fig. 9 presents some of these orbits in the phase space.

The term transient chaos is used to describe a chaotic-like response, which becomes periodic after some cycles. Therefore, under this condition, after a finite time, the orbit leaves the chaotic region, establishing a periodic or quasi-periodic motion [18]. Grebogi et al. [19] defines crises phenomenon as a collision between a chaotic attractor and a coexisting unstable fixed point or periodic orbit. The cited reference also argues that crises appear to be the cause of most sudden changes in chaotic dynamics. Therefore, transient chaos and crises are related. The nonlinear pendulum dynamics presents an interesting behavior related to this kind of behavior, and in order to analyze it, bifurcation diagram is revisited, enlarging a region related to transient chaos. Now, three different procedures are employed to construct two bifurcation diagrams. The first one considers similar initial conditions for each parameter value, neglecting the first 4000 periods (Fig. 10a). The second procedure neglects the first 150 periods considering the same initial conditions, which allows observing

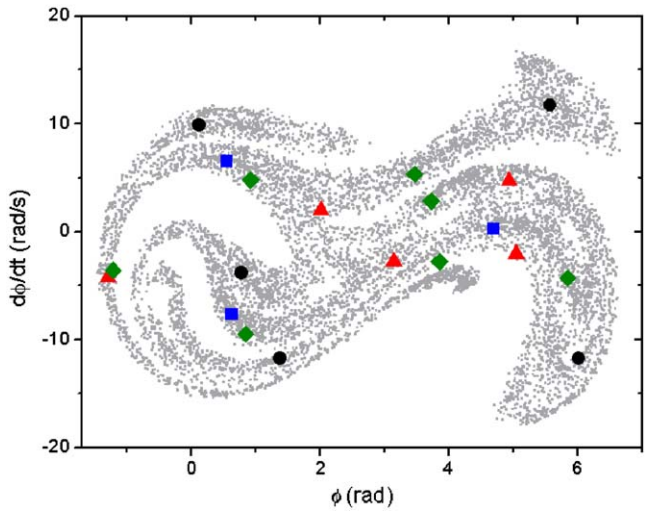

Fig. 8. Unstable periodic orbits embedded in strange attractor. ■ UPO period 3, ● UPO period 5, ▲ UPO period 5, ♦ UPO period 7.

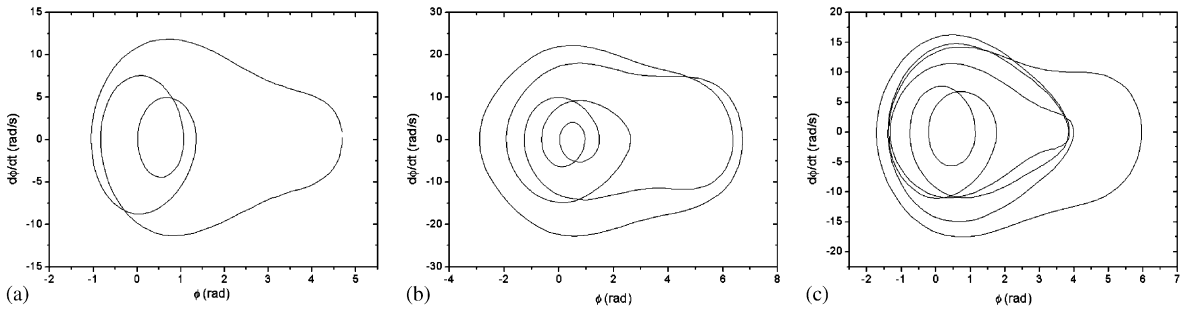

Fig. 9. Unstable periodic orbits: (a) period-3; (b) period-5; (c) period-7.

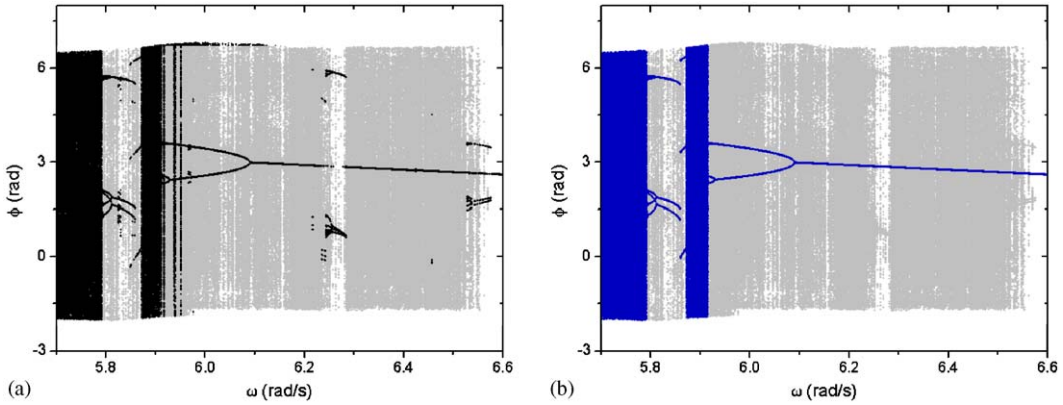

Fig. 10. Bifurcation diagram plotted by different procedures: (a) first and second procedures; (b) third and second procedures.

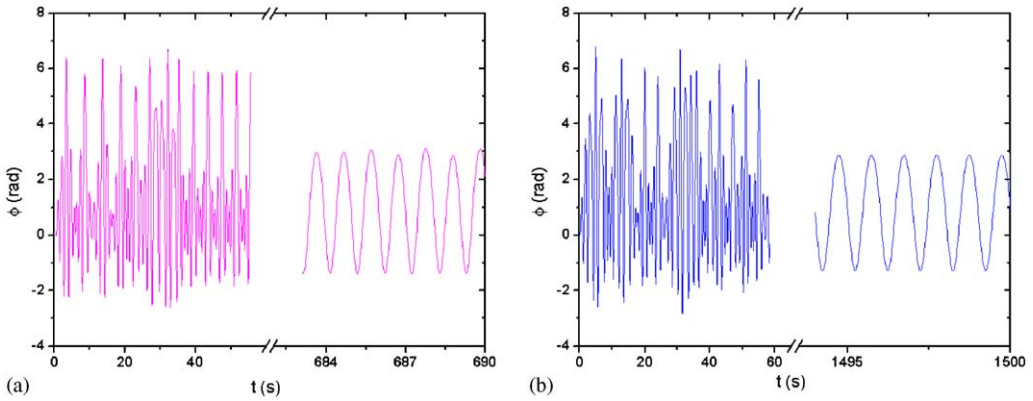

Fig. 11. Transient chaos: (a) experimental, (b) numerical.

part of the transient. The third procedure considers stabilized values of state variables as an initial condition for the next parameter value, neglecting 150 periods (Fig. 10b). The second procedure is shown in both diagrams allowing the transient chaos visualization, in background. Note that the third procedure is not able to capture neither the coexistence of different attractors nor the transient chaos.

Transient chaos is related to an irregular motion that tends to stabilize in a periodic motion after a long transient response. Fig. 11 presents both experimental and numerical results of this response for $\omega = 6.23\,\mathrm{rad/s}$. The analysis of Lyapunov exponents shows that the response presents a positive value that tends to become negative after the stabilization. During transient chaos, the spectrum is $\lambda = (+0.5, -0.6)$. However, in steady state, the spectrum is $\lambda = (-0.0323, -0.0914)$.

The transient chaos is also related to a fractal-like structure during the transient response, tending to be eliminated in the steady state. This is usually denominated chaotic saddle, being geometrically related to the strange attractor, but with repulsive characteristics. Fig. 12a shows this chaotic saddle and also the period-1 steady-state response. Fig. 12b, on the other hand, shows the period-1 steady-state orbit obtained either by numerical or by experimental approaches.

Another characteristic of the transient chaos is the sensitive dependence to initial conditions, which could be pointed out by some simulations. Fig. 13 presents simulations for $\omega = 6.23\,\mathrm{rad/s}$ and different initial conditions. At first, two different, very close, initial conditions are considered (Fig. 13a and b). These responses are related to the same steady-state orbit, which, presents a different transient response. By considering proper initial conditions, transient response can be eliminated. Fig. 13c shows a situation where

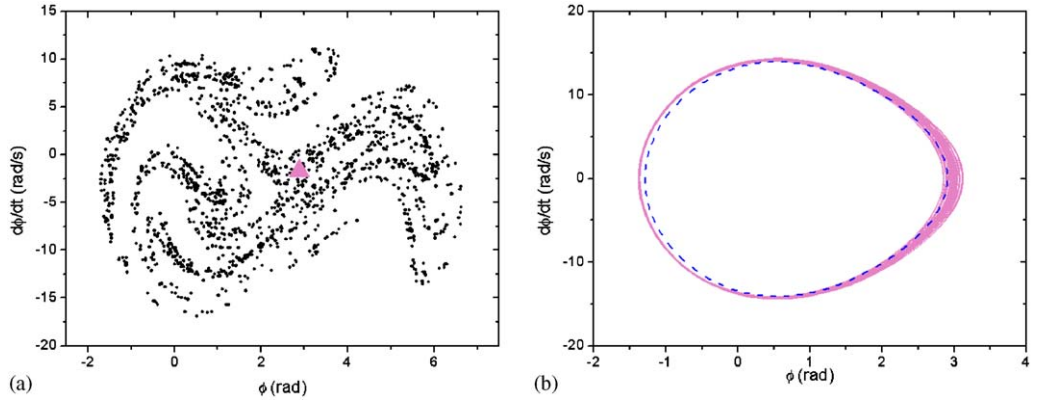

Fig. 12. (a) Chaotic saddle and the steady-state period-1 response; (b) period-1 steady state. — Experimental, - - - numerical.

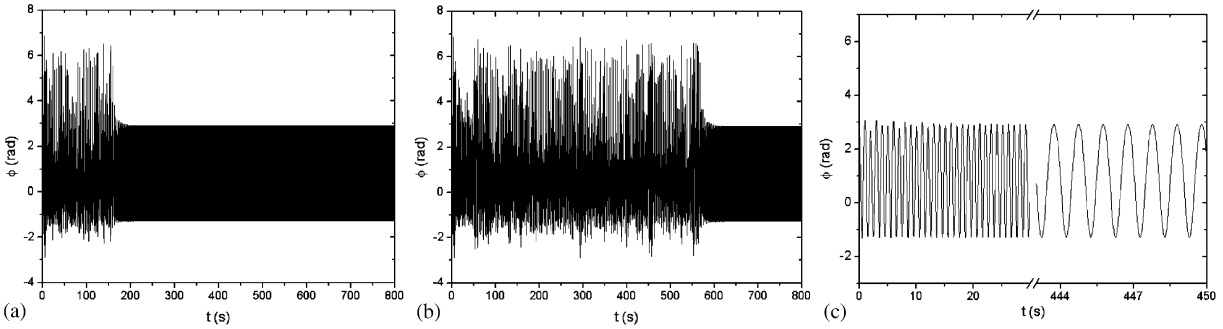

Fig. 13. Transient responses for different initial conditions: (a) $(\phi, \dot{\phi}) = (0.00293, 0.1421)$; (b) $(\phi, \dot{\phi}) = (0.00292, 0.14205)$; (c) $(\phi, \dot{\phi}) = (2.8, -2.2)$.

the steady-state orbit is achieved in the beginning of the motion. Similar situations could be seen in bifurcation diagrams. Therefore, it is possible to conclude that the existence of transient chaos depends on initial conditions.

By observing bifurcation diagram, there is a region related to the coexistence of stable attractors. Note that for $\omega < 6.235\,\mathrm{rad/s}$ or $\omega > 6.290\,\mathrm{rad/s}$ there is only a period-1 attractor. Other regions have different coexisting attractors. For example, when $\omega = 6.240\,\mathrm{rad/s}$, there are a period-4 and a period-1 coexisting attractors. A small change for $\omega = 6.245\,\mathrm{rad/s}$ may cause the appearance of three attractors: period-4, period-8 and period-1. By changing $\omega = 6.250\,\mathrm{rad/s}$, period-4 orbit disappears, remaining only period-8 and period-1 orbits. When $\omega = 6.250\,\mathrm{rad/s}$, period-4 orbit appears instead of period-8 orbit.

The coexistence of attractors may be assured constructing basins of attraction. For $\omega = 6.23\,\mathrm{rad/s}$, basins of attraction show just one steady-state orbit. However, by considering a different frequency parameter ($\omega = 6.28\,\mathrm{rad/s}$, for example), there are two coexisting attractors, as can be identified in bifurcation diagrams. The first one is a period-1 while the second corresponds to a period-4 response. Basins of attraction also illustrate this coexistence (Fig. 14). The dark color is associated with a period-4 response while the gray color is related to a period-1 response. For initial conditions in the neighborhood of the periodic attractors, period-1 or period-4, there is no transient chaos. On the other hand, the basins of attraction for regions far from the neighborhood of these points are mixed, being related to a transient chaos before the stabilization. Although these are not well-defined regions of initial conditions that lead to the periodic attractors in the mixed portion, roughly 75% of these initial conditions drive the system trajectory to the period-4 orbit. Fig. 15 shows both steady-state orbits obtained by numerical and experimental approaches.

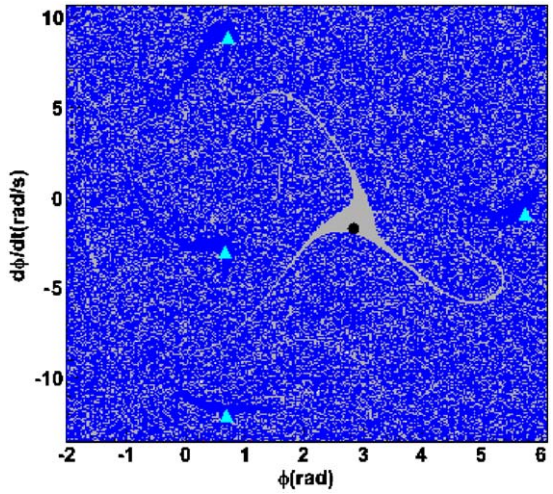

Fig. 14. Basins of attraction for $\omega = 6.28\,\mathrm{rad/s}$.

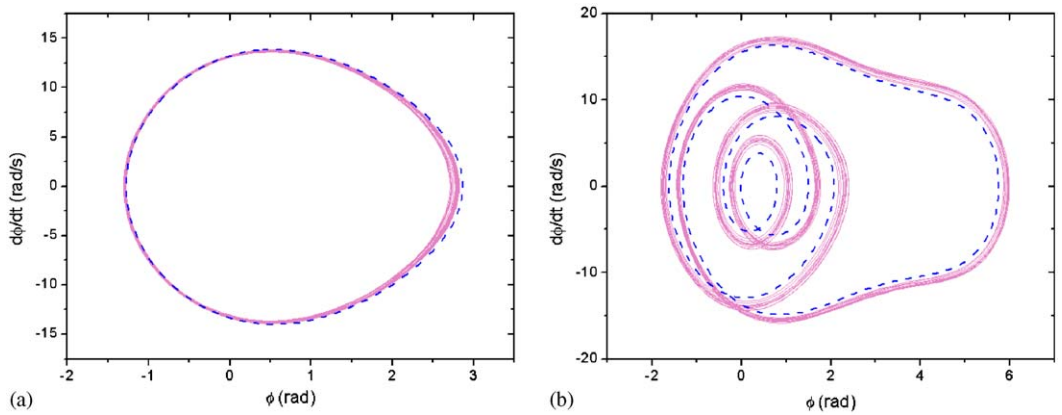

Fig. 15. Steady-state orbits, — experimental, --- numerical: (a) period-1 response; (b) period-4 response.

5. Conclusions

This contribution analyzes chaotic dynamics in an experimental nonlinear pendulum by both experimental and numerical approaches. The experimental apparatus has both torsional stiffness and damping, and is monitored with the aid of a rotary sensor. A mathematical model is proposed considering restoring and excitation forces, and also the dissipation process described by a combination of linear viscous damping and dry friction. After parameter identification, numerical simulations are carried out presenting close agreement with experimental data. The pendulum response is very rich presenting different kinds of response. Bifurcations, chaos and transient chaos are verified, exploiting different aspects of its nonlinear dynamics.

Acknowledgments

The authors would like to acknowledge the support of the Brazilian Research Council (CNPq). Moreover, the authors would like to thank Dr. Luiz Fernando P. Franca for his insightful comments in the beginning of this research.

References

[1] J.L. Trueba, J.P. Baltanás, M.A.F. Sanjuán, A generalized perturbed pendulum, *Chaos, Solitons and Fractals* 15 (2003) 911–924.
[2] L. Werner, T. Kurz, U. Parlitz, Experimental nonlinear physics, *Journal of the Franklin Institute* 334B (5/6) (1997) 865–907.
[3] J.A. Blackburn, G.L. Baker, A comparison of commercial chaotic pendulums, *American Journal of Physics* 66 (9) (1998) 821–829.
[4] D. D'Humieres, M.R. Beasley, B.A. Huberman, A. Libehaber, Chaotic states and routes to chaos in the forced pendulum, *Physical Review A* 26 (6) (1982) 3483–3496.
[5] T. Shinbrot, C. Grebogi, J. Wisdom, J.A. Yorke, Chaos in a double pendulum, *American Journal of Physics* 60 (6) (1992) 491–499.
[6] Q. Zhu, M. Ishitobi, Experimental study of chaos in a driven triple pendulum, *Journal of Sound and Vibration* 227 (1) (1999) 230–238.
[7] R. DeSerio, Chaotic pendulum: the complete attractor, *American Journal of Physics* 71 (3) (2003) 250–256.
[8] L.F.P. Franca, M.A. Savi, Distinguishing periodic and chaotic time series obtained from an experimental nonlinear pendulum, *Nonlinear Dynamics* 26 (3) (2001) 253–271.
[9] E.G.F. Pinto, M.A. Savi, Nonlinear prediction of time series obtained from an experimental pendulum, *Current Topics in Acoustical Research—Research Trends* 3 (2003) 151–162.
[10] F.H.I. Pereira-Pinto, A.M. Ferreira, M.A. Savi, Chaos control in a nonlinear pendulum using a semi-continuous method, *Chaos, Solitons and Fractals* 22 (3) (2004) 653–668.
[11] F.H.I. Pereira-Pinto, A.M. Ferreira, M.A. Savi, State space reconstruction using extended state observers to control chaos in a nonlinear pendulum, *International Journal of Bifurcation and Chaos* 15 (2005), in press.
[12] R.I. Leine, Bifurcations in Discontinuous Mechanical Systems of Filippov-type, Ph.D. Thesis, Technische Universiteit Eindhoven, 2000.
[13] A. Wolf, J.B. Swift, H.L. Swinney, J.A. Vastano, Determining Lyapunov exponents from a time series, *Physica D* 16 (1985) 285–317.
[14] C. Grebogi, E. Ott, S. Pelikan, J.A. Yorke, Strange attractors that are not chaotic, *Physica* 13D (1–2) (1984) 261–268.
[15] J. Guckenheimer, P. Holmes, *Nonlinear Oscillations, Dynamical Systems, and Bifurcations of Vector Fields*, Springer, Berlin, 1983.
[16] S. Wiggins, *Introduction to Applied Nonlinear Dynamical Systems and Chaos*, Springer, Berlin, 1990.
[17] D. Auerbach, P. Cvitanovic, J.-P. Eckmann, G. Gunaratne, I. Procaccia, Exploring chaotic motion through periodic orbits, *Physical Review Letters* 58 (23) (1987) 2387–2389.
[18] F.C. Moon, *Chaotic and Fractal Dynamics*, Wiley, New York, 1992.
[19] C. Grebogi, E. Ott, J.A. Yorke, Crises, sudden changes in chaotic attractors, and transient chaos, *Physica* 7D (1983) 181–200.